Composites Part B 223 (2021) 109122

Contents lists available at ScienceDirect

Composites Part B

journal homepage: www.elsevier.com/locate/compositesb

Processing and mechanical characterization of short carbon fiber-reinforced epoxy composites for material extrusion additive manufacturing

Nadim S. Hmeidat [a], Daniel S. Elkins [b], Hutchison R. Peter [c], Vipin Kumar [d], Brett G. Compton [a,e,*]

[a] Mechanical, Aerospace, and Biomedical Engineering Department, University of Tennessee, Knoxville, TN, 37996, USA
[b] Grado Department of Industrial and Systems Engineering, Virginia Tech, Blacksburg, VA, 24061, USA
[c] Department of Mechanical Engineering, Virginia Tech, Blacksburg, VA, 24061, USA
[d] Manufacturing Science Division, Oak Ridge National Laboratory (ORNL), Knoxville, TN, 37932, USA
[e] Material Science and Engineering Department, University of Tennessee, Knoxville, TN, 37996, USA

ARTICLE INFO

Keywords:
Additive manufacturing
3D printing
Extrusion
Direct ink writing
Short-fiber composites
Fiber length
Thermosets

ABSTRACT

Fiber-reinforced polymer composites have been extensively utilized in recent years as feedstock materials for material extrusion additive manufacturing (AM) processes to improve strength, stiffness, and functionality of printed parts over unfilled printed polymers. However, the widespread adoption of AM of fiber-reinforced polymer composites requires a deeper understanding of the process-structure-property relationships in printed components, and such relationships are not well understood yet. Fiber length is critically important to the mechanical performance of short fiber composites, but very few studies to-date have focused on how the fiber length distribution (FLD) evolves during processing of composite feedstocks and how this evolution affects printing behavior and mechanical properties in 3D-printed composites. In this work, FLD is measured for carbon fiber reinforced epoxy composites over a wide range of ink compositions and shear mixing times, and the distributions are fit with a Weibull-type distribution function. The effects of FLD on the tradeoff between ink processability, ink rheology, printing behavior and mechanical properties are investigated. Furthermore, the effects of printing parameters (nozzle size and print speed) on mechanical anisotropy and fiber orientation distribution (FOD) in printed composites are explored. Mechanical properties of printed composites are characterized via 3 pt-flexural testing, and microstructure is investigated using optical and scanning electron microscopy (SEM), and x-ray computed tomography. Finally, the fitted Weibull parameters are fed into a composite model that incorporates FLD and FOD, and model predictions are found to be in excellent agreement with experimental observations.

1. Introduction

Material extrusion additive manufacturing (AM) of polymer composites has been the focus of research interest in recent years for its unprecedented ability to create new structural components and multi-material architectures [1–6]. Extrusion-based AM methods consist of building components in a layer-by-layer format by selectively depositing material through a deposition nozzle [7]. Building components in this manner allows direct manufacture of complex structures that may not be feasible via traditional manufacturing approaches. Despite this unique flexibility, key challenges remain that hamper the widespread adoption of AM to produce robust, end-use structural components. Key challenges include: (1) the lack of feedstock materials with high specific properties and functionality that can compete with current engineering materials, (2) the associated printing-induced anisotropy and trapped porosity in printed parts, and (3) the lack of deep understanding of the process-structure-property relationships in additively manufactured parts.

A wide variety of polymer feedstock composites have been developed for material extrusion AM technologies – including fused filament fabrication (FFF) and direct ink writing (DIW) – utilizing different filler reinforcements in both thermoplastic and thermoset resins. For

* Corresponding author. Mechanical, Aerospace, and Biomedical Engineering Department, University of Tennessee, Knoxville, TN, 37996, USA.
E-mail address: bcompto1@utk.edu (B.G. Compton).

https://doi.org/10.1016/j.compositesb.2021.109122
Received 7 April 2021; Received in revised form 10 June 2021; Accepted 3 July 2021
Available online 8 July 2021

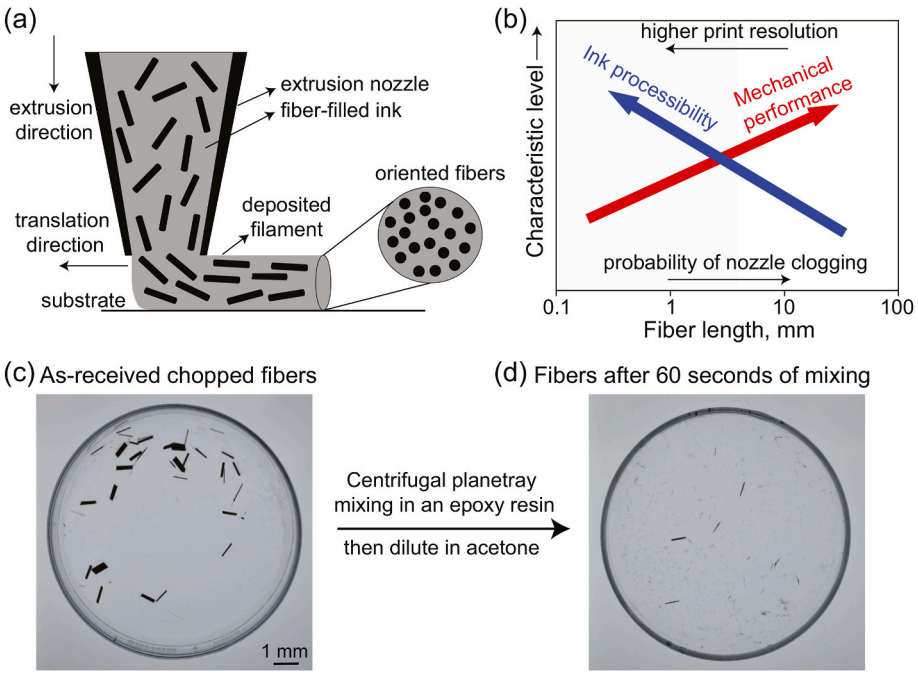

Fig. 1. Schematic illustrations of (a) direct ink writing (DIW) process, and (b) effect of fiber length on ink processability and mechanical performance in fiber-reinforced composites. The shaded area demonstrates a typical range of fiber lengths in short carbon-fiber composites, which exhibits an excellent combination of material processability and mechanical behavior. (c) and (d) show carbon fibers before and after mixing.

example, polymer feedstocks reinforced with carbon fibers (CFs) [8–16], glass fibers [17], silicon carbide microfibers [5,12,18,19], nanoclay [18, 20–23], graphene [24,25] and carbon and boron nitride nanotubes [26, 27] have been investigated to improve strength and stiffness in printed materials. Short fiber-reinforced polymer composites are of particular interest due to their combination of mechanical properties, low density, increased thermal stability, high processibility and low production cost [28,29]. Love et al. showed that the incorporation of CFs (up to 13 vol%) into a thermoplastic ABS resin could drastically diminish warping in printed parts by reducing the coefficient of thermal expansion (CTE) of neat ABS resin by 88.72% along the deposition direction [9]. The work also showed that printed ABS/CF composites exhibited higher tensile strength (~194% increase), stiffness (~335% increase), and thermal conductivity (~124.3% increase) than neat ABS when tested parallel to the deposition direction. Zhong et al. incorporated glass fibers (up to 18 wt%) into an ABS resin, leading to an increase of 140% in the tensile strength along the print direction; however, the presence of glass fibers was found to reduce the flexibility and robustness of the ABS filaments during handling [17]. Tekinalp et al. showed that short CFs align in the print direction during printing ABS/CF composites (up to 40 wt% CF), improving the strength by ~115% and the stiffness by ~700% along the print direction over neat ABS [10]. Although highly oriented CFs were achieved in printed ABS/CF composites, increased porosity caused lower tensile properties than those of their compression-molded counterparts [10]. It was also found that the average fiber length in printed ABS/CF composites decreased with increasing CF content, as a result of fiber breakage during compounding the CF and ABS resin under high-shear mixing [10]. Ning et al. investigated the effect of fiber length on the mechanical properties of ABS/CF composites printed via FFF at a CF loading of 5 wt% [30]. Their results showed that printed composites with fiber lengths of 150 μm achieved higher tensile strength and modulus than printed composites with fiber lengths of 100 μm [30].

Several short fiber-reinforced thermoset inks have been developed for DIW. For example, Calvert et al. were the first to use DIW for printing CF-reinforced epoxy composites in 1997 [31]. In that study, varying fractions of chopped CF with varying fiber lengths were utilized in epoxy resins in the presence of fumed silica (FS) to induce thixotropy. The modulus and strength of printed composites showed dependence on both fiber length and CF content, and fiber orientation was shown to follow the direction of printing [31]. In a subsequent study by Peng et al., flexural bars of epoxy/FS/glass-fibers were printed with varying print-head speeds and print paths (i.e. orientation angles) relative to the length of the bar [32]. Their results showed that the degree of fiber orientation increases with increasing print-head speed while keeping the flow rate constant. As a result of increased fiber alignment, the flexural modulus improved by 50% as the print-head speed increased by a factor of 2.5 [32]. More recently, Compton and Lewis showed that highly loaded epoxy/nanoclay/SiC/CF inks can reach Young's modulus values up to 24.5 GPa in the print direction [12], while Malek et al. achieved an elastic modulus up to 57 GPa in the print direction using pitch-based CFs in epoxy/nanoclay inks [33]. Nawafleh and Celik employed a vibration-assisted printhead to enable printing epoxy/NC/CF inks with a high CF content (up to 46 vol%), achieving flexural strength values up to 400 MPa and stiffness up to 53 GPa in the print direction [13]. Hmeidat et al. incorporated 15 vol% of SiC microfibers into an epoxy resin filled with either nanoclay (NC) or FS, achieving flexure strength values up to 215 MPa along the print direction [18]. In that study, the team also demonstrated that SiC microfibers become more highly aligned along the print direction when smaller deposition nozzles and higher print speeds are employed.

Along with printed short fiber-reinforced polymer composites, continuous fiber reinforced composites have also been successfully printed and characterized for material extrusion AM, using either thermoplastic [34–40] or thermoset [41,42] polymeric resins as the composite base. Although the mechanical properties of these printed composites are relatively higher than short fiber-reinforced polymer composites, AM of continuous fiber composites requires specialized hardware and is subject to some processing and geometric constraints that limit design freedom, such as minimal deposition height and minimal corner radii. The accessibility of printing short fiber composites – requiring only basic DIW or FFF hardware – and the fact that attractive properties have been demonstrated, motivate further study of printed short fiber composites, despite the superior properties found in continuous fiber composites.

Although most of the prior studies have shown significant advances in printed fiber-reinforced polymer composites with high mechanical properties, less attention has been given to the effect of formulation and processing parameters on the fiber length evolution in printed composites. The mechanical performance of short fiber composites is highly dependent on fiber content, fiber length distribution (FLD), fiber orientation distribution (FOD), and fiber-matrix interfacial adhesion [10,28,29]. Material extrusion AM is beneficial in this regard as it induces orientation of fibers as they are extruded through the deposition nozzle [10,12,14,18,31,32,43,44] (Fig. 1a). However, during formulating and printing of fiber feedstocks, fiber attrition can occur, affecting the rheological properties of the ink and the mechanical properties of printed composites [10,28,29]. To enable a better understanding of the mechanical behavior of printed short fiber composites, the linkage between fiber content, formulation processes, printing parameters, the resulting FLD and FOD, and mechanical properties of printed composites need to be established. Pierson et al. have investigated the effect of mixing time and fiber content (up to 5.5 vol%) on the FLD in epoxy/NC/CF inks for DIW [14]. Their results suggest that mean fiber length approaches a steady-state value above a certain mixing time for composite inks containing greater than 2.3 vol% carbon fibers. However, the team did not directly investigate how the mixing time and FLD affect rheological and mechanical properties.

This work seeks to better understand the evolution of fiber length during material processing, including how the FLD affects the tradeoff between processability (rheology and printing behavior, print quality), and mechanical properties (Fig. 1b). FLD are measured for a wide range of ink compositions and mixing times, and the distributions are fit with a Weibull-type distribution function. The fitted Weibull parameters are fed into a composite model developed by Fu and Lauke [28] that incorporates FLD and FOD, and model predictions are found to be in excellent agreement with experimental observations. In addition, the effect of nozzle size and print speed on mechanical anisotropy and fiber orientation in printed composites is investigated. Mechanical properties of printed composites are investigated via 3 pt-flexural testing, and microstructure is investigated using optical and scanning electron microscopy (SEM), and x-ray computed tomography (xCT). Results and insights gained from this work will enable the design of better composite feedstocks for material extrusion AM and more rigorous engineering design of printed composite components.

2. Experimental

2.1. Materials

EPON 826 (Momentive Specialty Chemicals, Inc., Columbus, OH) epoxy resin with a density of 1.162 g/cm^3, was utilized as the composite ink base. Dicyanex 1400 B (Evonik Industries AG, Essen, Germany), a dicyandiamide (DICY) powder, was employed as the latent curing agent for the epoxy resin. Kaltex K20-HTU carbon fibers (CF) from the Oak Ridge National Laboratory (ORNL) Carbon Fiber Technology Facility (CFTF) were used for this study [45]. These fibers are low-cost, PAN--derived fibers, sized for epoxy resin and chopped to 6 mm length with a density of 1.773 g/cm^3 (Fig. 1c and Fig. S1). Garamite-7305 nanoclay (NC) (BYK-Chemie GmbH, Wesel, Germany), with a density of 1.6 g/cm^3, was used to modify the viscosity of the resin and enhance the printing behavior. More information about the NC filler material can be found in Ref. [21].

2.2. Ink formulation

Inks were formulated using a centrifugal planetary mixer (FlackTeck, Inc., Landrun, SC) in 90-ml. plastic containers (FlackTeck, Inc., Landrun, SC). All batches were prepared using 20 g of epoxy resin. The fibers were added to the epoxy resin in different amounts, 3.1, 6.2, 9.15 and 12.2 vol %. After the addition of fibers, the inks were mixed for four different durations, 180, 360, 540, and 720 s, to observe the effects that the mixing process and fiber content have on the fiber length distribution. This resulted in a total of 16 different mixtures. Mixing was conducted under vacuum at 0.1 atm at a constant speed of 1800 rpm for all inks. Because high shear mixing can generate heat, the mixing time was divided into 180 s intervals to allow the mixer and ink to cool down. The cool-down period was ~10 min per interval. These ink formulations do not contain NC and will be referred to as the CF inks (Table 1). To identify any effects that the presence of the NC viscosity modifier has on fiber length evolution, an additional ink containing 9.15 vol% CF and 5 wt% (1.3 g) NC was formulated and mixed at the same aforementioned mixing times. The mixing was done in two steps to enable better dispersion of the fibers in the presence of NC. First, the CF was added and mixed for half of the targeted mixing period at 1800 rpm. Then, the NC was added and mixed at 1800 rpm. These formulations will be referred to as the CF/NC inks. After several trials, 5 wt% NC was identified as a suitable amount to modify ink viscosity and enable printing of self-supporting parts following [18]. Inks utilized for fiber length measurements did not contain any curing agent, but 1 g of DICY (corresponding to 5 parts per hundred by weight resin) was added into inks utilized for printing. In these inks, DICY was added to the epoxy resin before the fillers and was mixed under 0.1 atm for 60 s at a speed of 1500 rpm.

Table 1
Compositions of epoxy/CF ink formulations.

Resin (g)	CF (g)	CF (wt.%)	CF (vol%)
20	1	4.76	3.1
20	2	9.13	6.2
20	3.1	13.3	9.15[a]
20	4.24	17.5	12.1

[a] an additional ink was formulated at this fiber loading in the presence of 5 wt % NC filler.

Table 2
Volume-weighted average fiber length and Weibull distribution parameters for all inks formulated.

CF content (vol%)	Mixing time (seconds)	Sample size	Shape parameter, k	Scale parameter, λ (x10^{-6})	Volume-weighted average fiber length (mm)
3.1	180	419	1.852	664	0.587
	360	558	1.891	599	0.529
	540	240	1.901	576	0.526
	720	277	1.916	436	0.414
6.2	180	737	2.24	532	0.499
	360	808	2.18	441	0.389
	540	539	2.20	403	0.364
	720	362	2.30	316	0.287
9.15	180	1079	2.27	439	0.408
	360	709	2.27	361	0.317
	540	427	2.23	333	0.297
	720	288	2.30	296	0.268
12.1	180	973	2.25	466	0.455
	360	845	2.31	334	0.296
	540	183	2.10	279	0.248
	720	499	2.37	262	0.242
9.15 + 5 wt% NC	180	521	2.128	477	0.637
	360	520	2.564	374	0.344
	540	511	2.587	335	0.317
	720	511	2.583	302	0.280

2.3. Fiber length measurements

Fiber length measurements were taken for both CF and CF/NC inks. To reliably measure the variations in fiber lengths, the fibers must be separated from the epoxy matrix without altering length. Further, the fibers must all be aligned in a single plane. To do this, a stainless steel spatula was used to pull a small sample of material from the inks after each mixing cycle. The material was then placed in a bath of acetone to dissolve the epoxy. Then the specimen was immediately poured into a glass Petri dish so the acetone could evaporate. This process resulted in fibers that were oriented in single plane (Fig. 1d and Fig. S2). After the evaporation of acetone, the distributed fibers were imaged using a VHX-5000 digital microscope (KEYENCE Corporation, Itasca, IL), and the fiber lengths were measured manually. To develop greater confidence in the measurements, multiple images were stitched together to enable a larger number of full-length fibers to be measured. For the CF/NC inks, the acetone bath alone was insufficient to effectively separate the fibers from the epoxy/NC matrix. With the addition of NC, the fibers tend to form clumps of material, making it challenging to measure fiber lengths in the microscope. To solve this issue, the acetone bath was placed in a beaker inside an ultrasonic bath (Fisher Scientific, Waltham, MA) and sonicated for 3 min to force clumps of fibers to separate. Subsequently, the acetone bath was poured again into a Petri dish, and then immediately placed on a CIMAREC stirring hot plate (ThermoFisher Scientific, Waltham, MA) in a fume hood to expedite evaporation of the acetone. Then fiber length measurements were taken as described previously for the CF inks. The sample size of length measurements for each ink formulation is summarized in Table 2. It should be noted that all fiber length measurements were taken immediately after ink mixing; therefore, any potential fiber breakage due to loading the ink into the printer cartridge or during extrusion are not accounted for in the reported FLDs.

2.4. Ink rheology

Rheological properties were measured for the pure epoxy resin, epoxy/NC matrix and CF/NC inks, using a Discovery HR-2 Rheometer (TA Instruments, New Castle, DE) with 40 mm parallel platens for the pure resin and 25 mm parallel platens for all inks. To probe the effect of mixing time on ink rheology, inks with different mixing times were investigated. A gap size of 0.5 mm was used for both the pure epoxy resin and epoxy/NC inks, and a gap of 1.5 mm for the CF/NC inks. The apparent viscosity profiles were measured using continuous flow sweeps at controlled shear rates. The viscoelastic properties were measured using an oscillatory stress sweep at controlled oscillatory stresses with a frequency of 1 Hz. All measurements were preceded by a 120 s conditioning step at a constant shear rate of 0.01/s, followed by an equilibration period for 120 s. All tests were conducted at the ambient temperature of the lab (~21 °C).

2.5. 3D printing

Inks were loaded into 10 cm^3 syringe barrels (Nordson EFD, Westlake, OH) using a spatula. Loaded syringes were then centrifuged at 3900 rpm for 10 min using a Sorvall™ ST-8 Centrifuge (ThermoFisher Scientific, Waltham, MA), to get rid of any air bubbles that may have been introduced during ink loading, following [12,18,21]. The loaded syringe was then mounted on a custom 3-axis positioning stage (Shopbot Tools, Inc., Durham, NC) equipped with a pneumatic extrusion system for printing. The inks were printed onto substrates covered with polytetrafluoroethylene (PTFE)-coated aluminum foil (Bytac, Saint-Gobain Performance Plastics, Worcester, MA), to prevent permanent adhesion. Rectangular specimens were printed using tapered metal luer-lock nozzle tips (S-type, GPD, Grand Junction, CO) with three different inner diameters of 609, 864 and 1041 μm, and three translation print speeds of 10, 20 and 40 mm/s. The layer height and spacing between filaments were set as 0.6 and 0.8 times the inner diameter of the nozzle used, respectively. The extrusion pressure was adjusted manually to produce a flow-rate matched to the translation print speed (Table S1). Two print paths were employed to print mechanical test specimens, in which printed filaments (or roads) are either oriented parallel (hereafter referred to as longitudinal specimens) or orthogonal (hereafter referred to transverse specimens) to the length of the specimen (see Fig. S3). The g-codes were generated using custom programs written with Scilab software (Scilab Enterprises, Institut National de Recherche en Informatique et en Automatique, France). Following the printing process, all specimens were cured at 120 °C for 24 h, followed by 2 h at 220 °C. The density of the printed, cured specimens was measured using a Mettler Toledo Xs64 balance (Mettler-Toledo, LLC, Columbus, OH) equipped with an Archimedes density kit in distilled water.

2.6. Mechanical characterization

Flexural tests were performed at room temperature on an electromechanical load frame (Model 45, MTS Systems Corporation, Eden Prairie, MN, USA), using a load cell with a capacity of 1 kN. Flexural test specimens with nominal dimensions of 40 mm × 8 mm x 2 mm were tested in three-point flexure, using a span length of 32 mm and a crosshead speed of 0.8 mm/min. Edges and surfaces of the printed specimens were ground smooth prior to testing. Mechanical testing was performed according to ASTM D790 [46].

2.7. Microscopy

Optical micrographs were recorded using a VHX-5000 digital microscope (Keyence Corporation of America, Itasca, IL), to observe features of as-printed specimens, fiber lengths and fracture surfaces. Additionally, scanning electron microscopy (SEM) was carried out on a Phenom Desktop microscope (Nanoscience Instruments, Inc, Phoenix, AZ), to observe the morphology of the as-received carbon fibers, as well as select fracture surfaces of tested CF/NC flexural specimens. All observed specimens were sputter-coated with gold prior to SEM imaging.

2.8. X-ray computed tomography

xCT scans were conducted on 3D printed CF/NC composites using a ZEISS Xradia Versa 520 xCT equipment. Two specimens were measured, one using the highest print speed and one using the lowest print speed, and were taken from flexural test specimens. The xCT data were collected at 3 W power and 40 kV accelerating voltage. Tomographs of the middle section of the tested composites (a cylinder with 2 mm diameter and 2 mm height) were recorded. For each tomogram, 1 μm resolution was maintained to capture the individual CFs. A 4× scintillator objective attached with a Charged Coupled Device (CCD) camera was used to record the scans. The recorded scans were visualized using the image processing software Avizo (version 9.3.0, XFiber module, ThermoFisher Scientific), and the Xfiber extension was used to quantify the FODs [47,48]. The Xfiber extension provides tools to trace the centerlines of cylindrical features. A detailed workflow of the analysis is given in Ref. [49]. Using an assumed minimum fiber length and fiber radius, the analysis enables the construction of a fiber orientation tensor representing the local distribution of the fibers. A spherical coordinate system was used to describe the fiber orientation, with theta (θ) representing the offset angle between the fiber axis and the Z-axis (which is the printing direction in the present work). θ varies in the range of 0°–90°, and fibers are considered aligned to the print direction when θ approaches 0°.

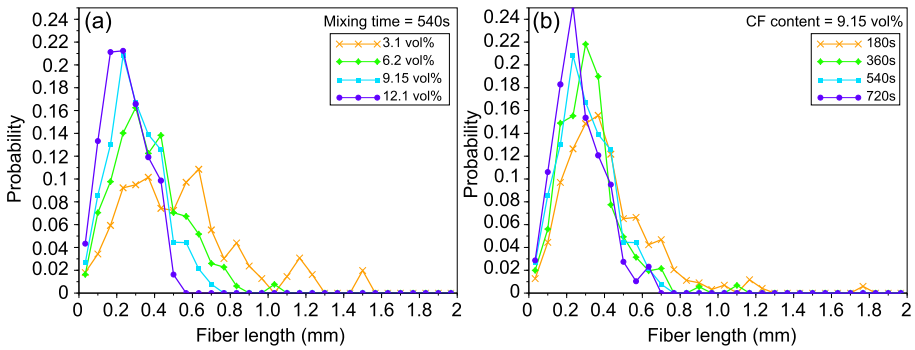

Fig. 2. Fiber length evolution during processing of CF inks: (a) FLDs for inks with different CF contents mixed for one mixing time (540s) and (b) FLDs for inks with constant CF content (9.15 vol%) mixed for different times.

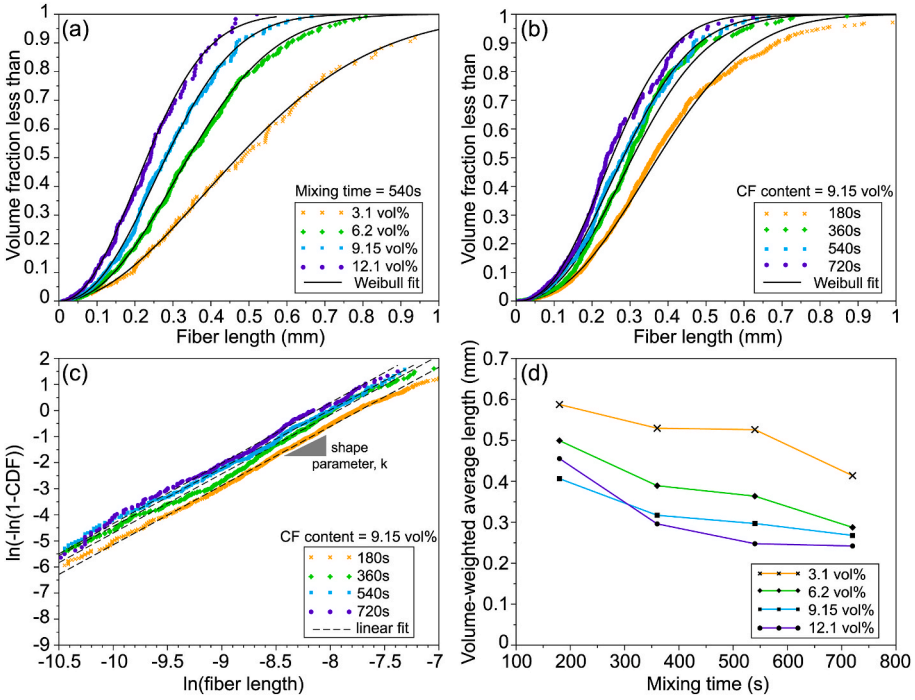

Fig. 3. (a–b) CDFs of the corresponding FLDs shown in Fig. 1a and b, respectively, along with fitted Weibull distributions (solid lines). (c) Weibull fit parameters computation (Eq. (1)) for inks with constant CF content of 9.15 vol% mixed for different times, along with dashed lines representing the linear regression of each dataset. (d) A summary of volume-weighted average fiber length values in all CF inks for different mixing times and CF contents.

3. Results and discussion

3.1. Fiber length evolution in CF inks

The effects of CF content and mixing time on the fiber length distribution (FLD) during ink processing are illustrated in Fig. 2. The FLDs shown are the volume-weighted fiber length probability histograms of the fiber length data, plotted using 30 bins over a length range from zero to two mm, corresponding to a bin width of 0.0667 mm. The volume-weighted distribution is used because it is the volume fraction of fibers at a given length, rather than the number of fibers, that dictate mechanical properties in the composite. The volume-weighted distribution is given by multiplying the number of fibers in each bin by the fiber length represented by that bin. Fig. 2a shows the FLDs for inks with different CF contents mixed for one mixing time (540s), while Fig. 2b shows normalized FLDs for inks with constant CF content (9.15 vol%) mixed for different times. In both cases, the mixing process results in asymmetrical FLDs. No fibers above 2 mm in length were observed. The most probable fiber length decreases with increasing CF content and with increasing mixing time, as indicated by a peak shift and narrower distributions with increasing mixing time or fiber content. Fiber breakage may occur as a result of the interactions between fibers during the high-shear mixing process, interactions between fibers and the resin, and interaction between the fibers and surfaces of the mixing container. Increasing fiber content and mixing time increases the number of fiber interactions, leading to increased fiber breakage and shorter fibers in the resulting ink formulation.

A two-parameter Weibull distribution function can be employed to model the FLD for each parameter set [28,50–52]. The cumulative distribution function (CDF) is given as [28]:

$$CDF = 1 - exp\left[-\left(\frac{L}{\lambda}\right)^{k}\right] \quad (1)$$

where L is the fiber length, λ and k are the scale and shape parameters of the Weibull distribution, respectively. Fig. 3a and b shows the experimental CDFs (dotted lines) of the corresponding FLDs in Fig. 2a and b, respectively, along with the Weibull fitted CDF curves (solid lines). The

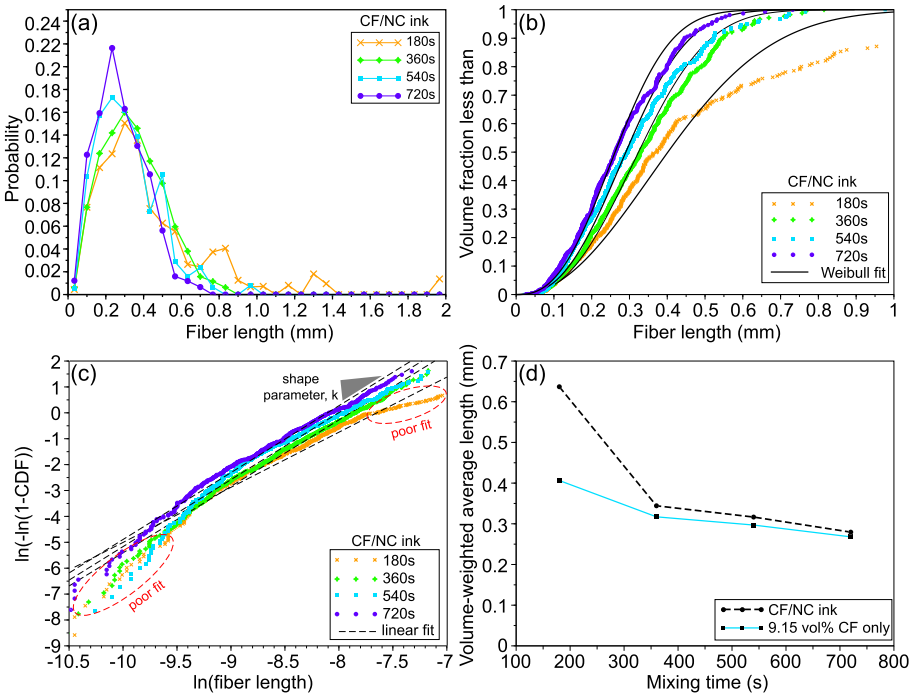

Fig. 4. Fiber length evolution during processing of CF/NC inks: (a) FLDs for CF/NC inks mixed for different times, (b) CDFs of the corresponding FLDs shown in (a), along with fitted Weibull distributions (solid lines). (c) Weibull fit parameters computation (Eq. (1)) for the CF/NC inks mixed for different times, along with dashed lines representing the linear regression of each dataset. (d) A comparison between the volume-weighted average fiber lengths measured for inks containing 9.15 vol% CF and mixed for different times, in the presence and absence of NC.

corresponding Weibull-fitted probability distribution curves (using equation s(1)) are displayed in Fig. S4a and S4b, respectively. The CDF curves shift upward and to the left (i.e. towards shorter fiber lengths) with increasing fiber content and increasing mixing time, without considerably changing the nature of the curves. The Weibull parameters are computed from the experimental CDF curves by linear regression on a double log-log plot, as illustrated in Fig. 3c for the ink containing 9.15 vol% CF.

Comparing the Weibull-fitted CDF curves with the experimental CDF data reveals a reasonably good fit across all parameter sets. Interestingly, all length data sets have a similar shape parameter, k, which ranges from ~2 to ~2.3, while the scale parameter, λ, decreases systematically with increasing CF content and mixing time. The computed Weibull parameters for all inks tested are summarized in Table 2.

The measured volume-weighted average fiber lengths for all sample sets are plotted in Fig. 3d. The initial fiber length (6 mm) was reduced to an average fiber length value below 0.6 mm across all CF contents and mixing times probed. This behavior indicates that high-aspect-ratio carbon fibers fracture easily during the shear mixing process, even at low CF contents and low mixing times. The volume-weighted average fiber length appears to reach a steady state value of ~0.27 mm for high fiber content and long mixing time, in broad agreement with the mean fiber lengths reported by Pierson et al. [14]. All volume-weighted average fiber length values for all CF inks tested are summarized in Table 2.

3.2. Fiber length evolution in CF/NC inks

The incorporation of NC results in higher viscosity of the carrier resin, which is expected to influence the FLD. Fig. 4a presents the FLD of the CF/NC ink containing 9.15 vol% CF at different mixing times, and Fig. S4c presents the corresponding Weibull-fitted probability distribution curves. Changing the rheology of the carrier resin by adding NC leads to noticeable differences in FLD compared with the CF inks, particularly at low mixing times. At a mixing time of 180 s, a poor Weibull fit is obtained (Fig. 4b) as compared to the same mixing time without NC (Fig. 3b). However, as mixing time increases with NC, the FLD adopts a more Weibull-like distribution.

FLDs in the presence of NC are plotted in Fig. 4c on double log-log axes to enable fitting of Weibull parameters to the data. Poor fit in the lower region of the plot indicates that the presence of NC reduces the number of very short fibers, whereas the poor fit in the upper region indicates a higher number of long fibers. A comparison of the average fiber lengths as a function of mixing time for the 9.15 vol% CF inks with

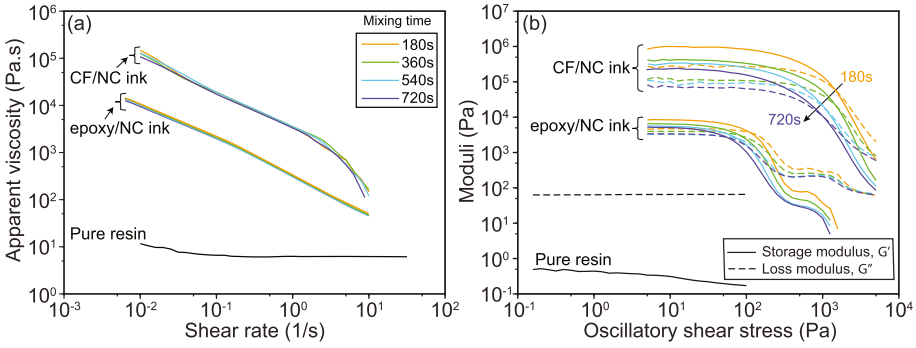

Fig. 5. Rheological behavior of epoxy-filled inks as a function of mixing time. (a) Log-log plots of apparent viscosity as a function of shear rate. (b) The corresponding storage and loss moduli as a function of oscillatory shear stress for the inks shown in (a).

Table 3
Effect of mixing time on the rheological properties of epoxy/NC and epoxy/CF/NC inks.

	epoxy/NC ink				CF/NC ink			
Mixing time (s)	n	K $(Pa.s^n)$	$G_0^{'}$ (kPa)	τ_y (Pa)	n	K $(Pa.s^n)$	$G_0^{'}$ (kPa)	τ_y (Pa)
180	0.254	372.3	8.443	113.3	0.188	3423.7	956.2	1519
360	0.250	352.2	6.513	82.6	0.237	3357.7	414.5	1516
540	0.250	336.5	5.614	77.0	0.212	3344.7	334.0	1101
720	0.266	343.8	5.150	56.3	0.230	3178.7	223.7	1015

and without NC is shown in Fig. 4d. The results show that, after a sufficient mixing time, the effect of NC diminishes, and average fiber lengths converge. The computed Weibull parameters, as well as the average fiber length values for all the CF/NC inks are summarized in Table 2. These observations can provide useful guidance on developing better CF-based inks using tailored compositions and mixing protocols.

3.3. Rheological behavior

The rheological behavior of epoxy-based inks of varying compositions and mixing times are shown in Fig. 5. The unfilled epoxy resin exhibits a Newtonian behavior with a viscosity of $\sim 10\ Pa.s$ that is nominally independent of shear rate over the range probed (Fig. 5a). The incorporation of NC platelets significantly increases the viscosity of the base resin by up to three orders of magnitude at low shear rates. However, as the shear rate increases, the viscosity decreases by several orders of magnitude, undergoing strong shear-thinning behavior. This phenomenon is important to facilitate extrusion of highly loaded inks. Upon the incorporation of 9.15 vol% CF, the CF/NC ink exhibits a viscosity that is only an order of magnitude higher than that of the epoxy/NC ink at any given shear rate below $\sim 8\ s^{-1}$, without changing its shear-thinning behavior.

Additionally, it is apparent that the mixing time does not have an impact on the viscosity profile of the epoxy/NC inks with and without CF, as they display similar apparent viscosities and shear-thinning behavior for all mixing times. The shear-thinning behavior can be quantified by fitting the apparent viscosity vs shear rate curves in Fig. 5a–a standard power law flow model of the form [21]:

$$\eta = K\,\dot{\gamma}^{n-1} \tag{2}$$

where η is the apparent viscosity, $\dot{\gamma}$ is the shear rate, K is the consistency index and n is the flow index. n and K values were computed by linear regression over the range from 0.01 to 1 s^{-1} for all inks. n values range from 0.25 to 0.266 for the epoxy/NC inks, and from 0.188 to 0.237 for the CF/NC inks. These values indicate good shear-thinning behavior, and they fall within the range of many successful DIW inks reported in literature [12,18,21,24,53,54]. The consistency index was also computed for these inks. Table 3 summarizes the numerical values computed for both n and K.

Plots of the storage ($G^{'}$) and loss ($G^{''}$) moduli of the corresponding inks are shown in Fig. 5b. The pure resin exhibits a storage modulus ($G^{'}$) that is about two orders of magnitude lower than its loss modulus ($G^{''}$), and both moduli are nearly independent of the applied oscillatory shear

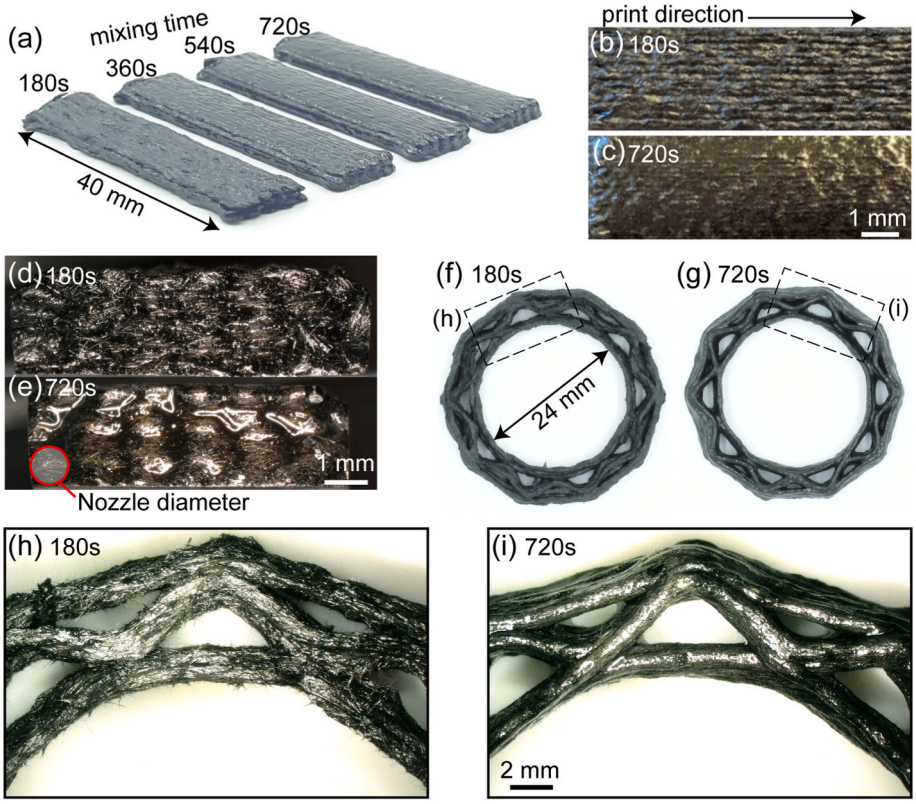

Fig. 6. (a) Representative optical micrographs of as-printed CF/NC longitudinal flexural test specimens. (b and c) Top-view optical micrographs of as-printed longitudinal specimens for mixing times of 180 s and 720 s, as well as (d and e) end views of the same bars, and (f–i) optical micrographs of printed complex geometries for the same mixing times of 180 s and 720 s.

stress, indicating a liquid-like material. Upon the addition of filler materials to the pure resin, both moduli increase considerably for all inks. Inks exhibit predominantly solid-like behavior at low shear stresses, where $G' > G''$, with a well-defined shear yield stress, τ_y, represented here by the crossover point between the two moduli. At shear stresses greater than the yield stress, the ink behaves predominantly as a liquid. In contrast to the shear-thinning behavior (Fig. 5a), the mixing time has a strong effect on the viscoelastic properties of the inks, where the storage and loss moduli and the shear yield stress are observed to decrease with increased mixing time (Fig. 5b). The presence of CF leads to more pronounced dependence on mixing time. The steady-state, stress-independent value of the storage modulus curve before yielding ($G' > G''$) is referred to as the equilibrium storage modulus (G'_0). The CF/NC ink displays higher G'_0 and τ_y values than the epoxy/NC ink across the different mixing times and G'_0 and τ_y values for each ink are summarized in Table 3.

The decrease in the elastic stiffness and shear yield stress of these inks with mixing time may be attributed to variations in the degree of NC exfoliation and CF length and dispersion within the epoxy resin. The shear-mixing process was reported to improve the degree of dispersion and exfoliation of filler materials within base polymers [55,56]. At low mixing times, longer fibers tend to entangle and bundle, and the probability of the presence of non-exfoliated agglomerates of NC increases [55,57]. This, in turn, can result in stiff inks that require higher extrusion pressure – due to the associated high shear yield stress – to enable flow through a given nozzle diameter. However, at higher mixing times, shorter fibers can disperse more easily throughout the carrier resin with less entanglement and the resin can intercalate between the NC platelets to exfoliate them to a higher degree [56,58].

3.4. Printing behavior

Through a series of extrusion and printing tests, it was observed that inks containing CF alone (without NC) did not possess sufficiently solid-like behavior and viscosity to enable printing self-stable parts. In addition, they were not able to be extruded reliably without frequently clogging the deposition nozzle, as fibers tend to entangle as they approach the nozzle exit [59]. In contrast, favorable printing behavior was obtained with the CF/NC inks. Fig. 6a shows representative, as-printed flexural specimens printed with the CF/NC ink at varying mixing times. These inks were extruded reliably through a 864-micron-diameter nozzle at and below an extrusion pressure of 1186 kPa (172 psi) without fiber clogging. As mixing time increased, a lower pressure value was required to extrude the ink as a result of the decreased yield stress. The extrusion pressure values for the CF/NC ink as a function of mixing time are summarized in Table S1. Moreover, all CF/NC inks were able to recover sufficient solid-like behavior after deposition, enabling flexural test specimens to be printed with minimal material spreading (Fig. 6a). However, poor print quality is observed at the lowest mixing time.

Optical images of representative as-printed samples are shown in Fig. 6 for the lowest and highest mixing times. Although the same nozzle size and CF content are employed, the mixing time along with the resulting FLD has a significant effect on the surface character and the quality of the printed part. At the lowest mixing time (180 s) (Fig. 6b,d,f,h), the surface features are rough and irregular and individual fibers can be seen protruding from the printed material (Fig. 6h). In contrast, at the highest mixing time (720 s) (Fig. 6c,e,g,i), the as-printed surfaces are smooth, without any fibers protruding, and the printed lines appear to be mostly coalesced, potentially leading to better adhesion of the epoxy matrix between adjacent filaments compared to the mixing time of 180 s.

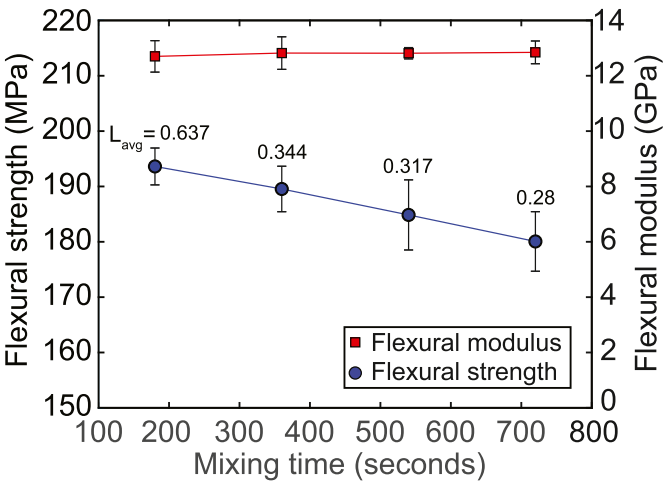

Fig. 7. Flexural strength and stiffness of 3D-printed CF/NC longitudinal specimens as a function of mixing time.

3.5. Mechanical behavior vs. mixing time

The flexural strength and flexural modulus for unidirectional composites tested along the print direction are shown in Fig. 7 for various mixing times and numerical values are summarized in Table 4. Flexural strength decreases monotonically with increasing mixing time from 193.6 MPa down to 180.1 MPa for mixing times of 180s and 720s, respectively (Fig. 7). This is consistent with composite theory that predicts higher composite strength with longer fibers [29]. However, flexural modulus values are not influenced by mixing time, with values ranging from 12.7 to 12.85 GPa. Although tensile characterization was not performed in this study, Pierson et al. (2019) [14] performed both flexural and tensile characterization of very similar 3D-printed short carbon fiber reinforced epoxy composites. For their printed composite most similar in fiber content to the present formulation, they found the tensile elastic modulus to be ~10% higher than the flexural modulus and the tensile strength to be ~75% that of the flexural strength [14]. These observations are consistent with composite theory for anisotropic, brittle materials and similar trends would be expected with the printed composites studied here.

3.6. Microscopy

Optical micrographs of representative fracture planes for longitudinal specimens are shown in Fig. 8., looking parallel to the fracture plane (Fig. 8a–d) and normal to the fracture plane (Fig. 8e–h). In the parallel views, fiber pull-out is clearly visible, and the fibers are predominantly oriented along the print direction. In addition, variations in the pull-out lengths of the fibers can be observed for the different mixing times, with longer fiber pull-out lengths corresponding to the lowest mixing time (180 s) and progressively shorter pull-out length with increasing mixing time (Fig. 8a–d), consistent with the variations in the average fiber length measured for each case.

Looking normal to the fracture plane, the fracture surface for the 180-s sample has a rougher appearance compared to the other fracture surfaces (Fig. 8e), indicating a higher crack bifurcation rate and higher energy consumption achieved with longer fibers during fracture. Moreover, interfaces between individual filaments are not apparent in any of the fracture surfaces, and there is no delamination observed between printed layers, indicating strong matrix bonding throughout the bulk of the specimens. However, a small amount of porosity (indicated with yellow arrows) exists within the printed specimens for the lower two mixing times (Fig. 8e and f). Fig. S5 displays higher magnification optical micrographs of the observed porosity. This porosity is attributed to the longer fibers that are more prone to forming fiber bundles and

Table 4
Flexural properties of printed epoxy/CF/NC composites at different mixing times and print parameters.

Mixing time (sec)	Nozzle size, D(mm)	Print speed, ν (mm/s)	$\nu/D(1/s)$	Print path*	Flexural modulus (GPa)	Flexural strength (MPa)	Strain-to-failure (%)	Number of specimens
180	0.864	40	46.3	L	12.70 ± 0.57	193.6 ± 3.3	1.60 ± 0.07	7
360	0.864	40	46.3	L	12.82 ± 0.60	189.5 ± 4.1	1.68 ± 0.08	8
540	0.864	40	46.3	L	12.81 ± 0.21	184.9 ± 6.3	1.60 ± 0.11	10
720	0.864	40	46.3	L	12.85 ± 0.41	180.1 ± 5.4	1.65 ± 0.05	8
				T	4.67 ± 0.09	88.5 ± 5.4	2.68 ± 0.24	4
720	0.864	20	23.1	L	12.65 ± 0.32	169.8 ± 6.5	1.52 ± 0.10	5
				T	4.77 ± 0.24	92.6 ± 7.5	2.80 ± 0.42	4
720	0.609	40	65.7	L	13.02 ± 0.70	190.7 ± 4.4	1.58 ± 0.08	5
				T	4.69 ± 0.35	88.3 ± 9.5	2.75 ± 0.45	4
720	1.041	40	38.4	L	12.80 ± 0.46	177.7 ± 4.1	1.60 ± 0.07	6
				T	4.76 ± 0.15	90.2 ± 8.9	2.65 ± 0.27	4
720	1.041	10	9.6	L	12.57 ± 0.23	155.3 ± 9.0	1.15 ± 0.12	4
				T	4.92 ± 0.48	99.3 ± 5.0	2.75 ± 0.19	4

L: longitudinal; T: transverse.

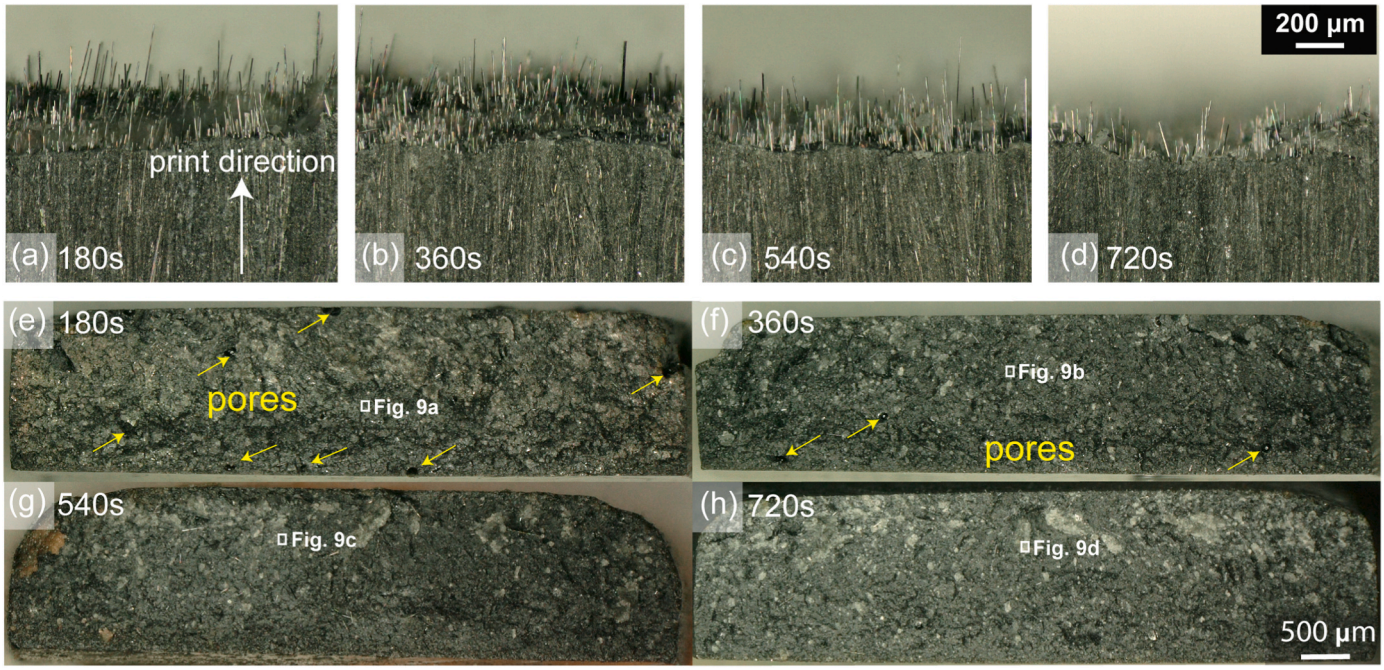

Fig. 8. (a–d) Representative optical micrographs of the parallel-views of fracture surfaces for CF/NC longitudinal specimens showing variations in the pull-out lengths. (e–h) Representative optical micrographs of the end-views of the corresponding fracture surfaces shown in (a–d).

inhibiting complete dispersion. With air pressure extrusion, even though no clogging was observed with the inks of low mixing times, the variation in fiber dispersion can cause uneven flowrate as the fiber bundles pass through the nozzle, which can lead to void formation. Part of the observed porosity could result from entrapped air pockets in the ink, introduced during loading the inks into the syringe, also leading to discontinuities during printing. Measured density values corroborate the increase in observed porosity with decreasing mixing time, as the density of the printed specimens increases from 1.248 ± 0.01 g/cm^3 to 1.262 ± 0.003 g/cm^3 as mixing time increases from 180 s to 720 s (Fig. S6).

Fig. 9 displays representative SEM images of the select points on the fracture surfaces (indicated with white squares in Fig. 8e–h). Fiber pull-outs are visible as exposed fibers or heart-shaped voids, matching the shape of the fiber cross-sections, distributed within the epoxy/NC matrix. It is noteworthy that the number of fibers that have been pulled from the fracture surface appears to increase with mixing time. This may be a result of the fact that a higher proportion of fibers are below the critical fiber length – discussed in the following section – with increased mixing time.

3.7. Mechanical property prediction vs. mixing time

Fu and Lauke proposed a modified rule-of-mixtures composite model that incorporates the effects of a realistic FLD and FOD on the composite strength through a fiber orientation factor and fiber length factor [28,60]:

$$\sigma_{cu} = \chi_1 \chi_2 \sigma_{fu} V_f + \sigma_m V_m \quad (3)$$

where χ_1 is the fiber orientation factor, χ_2 is the fiber length factor, V_f is the volume fraction of fibers within the composite, σ_{fu} is the ultimate strength of the fiber, V_m is the volume fraction of the matrix, and σ_m is the strength of the matrix. This model has proven successful in predicting the mechanical properties of short fiber composites fabricated via extrusion and injection molding processes [28,60]. More recently, Van de Werken et al. have validated the suitability of the model for predicting the strength and modulus of 3D-printed short-fiber thermoplastic composites with varying CF contents [11]. In the following

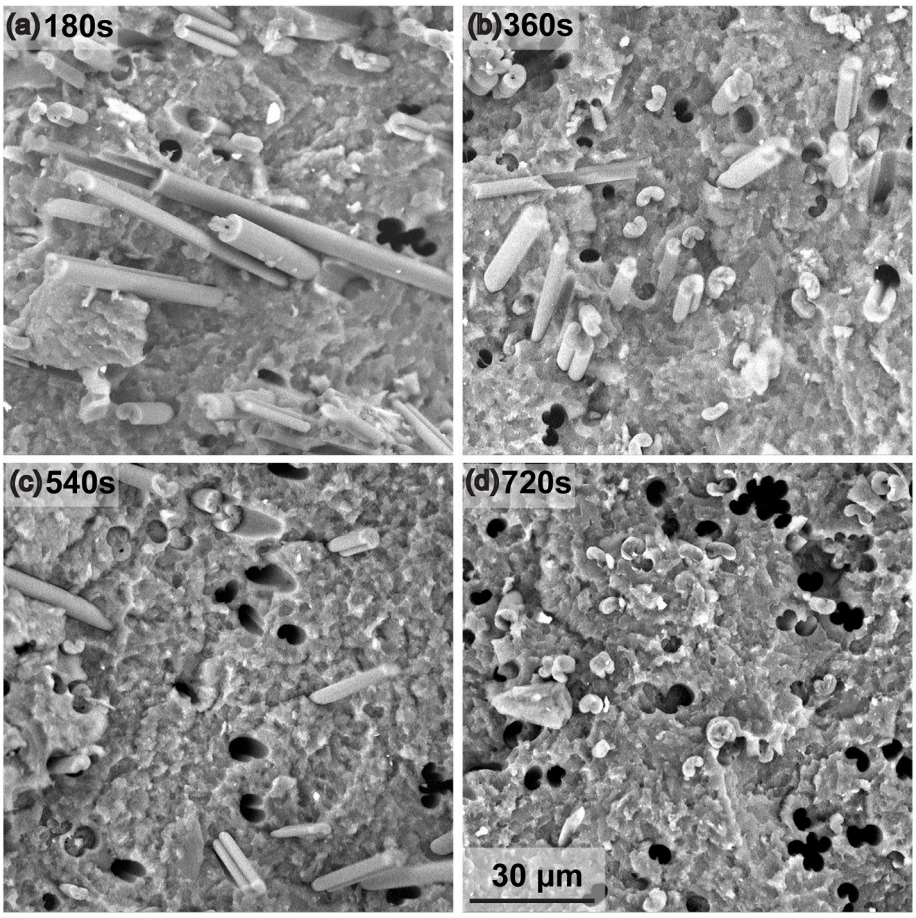

Fig. 9. Representative SEM micrographs of selected fracture surfaces for CF/NC unidirectional flexural specimens printed with varying mixing times: (a) 180 s, (b) 360 s, (c) 540 s and (d) 720 s. Black voids in the fracture surfaces are the holes that result from fiber pullout.

section this model is assessed against the printed composites studied here, using their measured FLD.

For unidirectional composites with fibers perfectly oriented parallel to the loading direction, $\chi_1 = 1$ [28]. In 3D-printed short fiber composites, alignment is not perfect and has been shown to depend on deposition nozzle size, print speed, and fiber content [10,18,32]. In the present set of experiments, because the nozzle size, print speed, and fiber content were held constant, χ_1 is assumed to adopt a constant value. On the other hand, χ_2 is expected to decrease with decreasing average fiber length or increasing mixing time. χ_2 can be directly calculated as:

$$\chi_2 = \int_{L_{min}}^{L_c} \left[L^2 / \left(2L_c L_{average}\right)\right] f(L)dL + \int_{L_c}^{L_{max}} \left(L / L_{average}\right)\left(1 - L_c / 2L\right) f(L)dL \tag{4}$$

where $L_{average}$ is the average fiber length, L_c is the critical fiber length, and $f(L)$ is a version of the Weibull distribution, known as the Tung distribution [28,50]::

$$f(L) = abL^{b-1}\ exp\left[-aL^b\right] \tag{5}$$

where $a = \lambda^{-k}$, $b = k$, and λ and k are the scale and shape parameters of the Weibull distribution described in section 3.1. The critical fiber length, (L_c) – the minimum fiber length required to transfer sufficient load from the matrix to the fiber for fiber fracture to occur – can be defined as [28,29]:

$$L_c = \frac{r_f\ \sigma_{fu}}{\tau_i} \tag{6}$$

where r_f is the fiber radius and τ_i is the interfacial shear strength between fiber and matrix. τ_i can be approximated by assuming that the interfacial shear strength is equal to the shear strength of the matrix. Assuming yield occurs according to the Tresca yield criterion:

$$\tau_i = \frac{\sigma_m}{2} \tag{7}$$

where $\sigma_m$is given as 100 MPa for the epoxy/NC matrix, following [21]. Therefore, from equation (6), the estimated value of L_c is 0.275 mm. Table 5 summarizes the mechanical properties of the fiber and matrix constituents.

Combing the preceding equations, the following equation is obtained:

Table 5
Properties of composite components.

Property	Value	Unit
Fiber ultimate strength, σ_{fu}	2750	MPa
Fiber elastic modulus, E_f	275.1	GPa
Fiber initial length, L_i	~6	mm
Fiber critical length, L_c	0.275	mm
Fiber radius, r_f	~5	μm
Matrix ultimate strength, σ_m	100[a]	MPa
Matrix elastic modulus, E_m	3.24[a]	GPa
Interfacial shear strength, τ_i	50[a]	MPa

[a] For the epoxy/NC base ink (5 wt% NC).

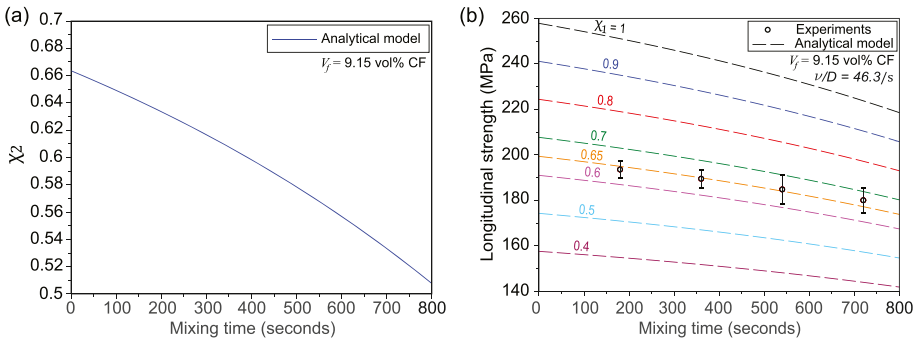

Fig. 10. (a) χ_2 as a function of mixing time, and (b) model predictions (dashed lines) of the longitudinal composite strength as a function of mixing time and χ_1 value, plotted along with the experimental strength values.

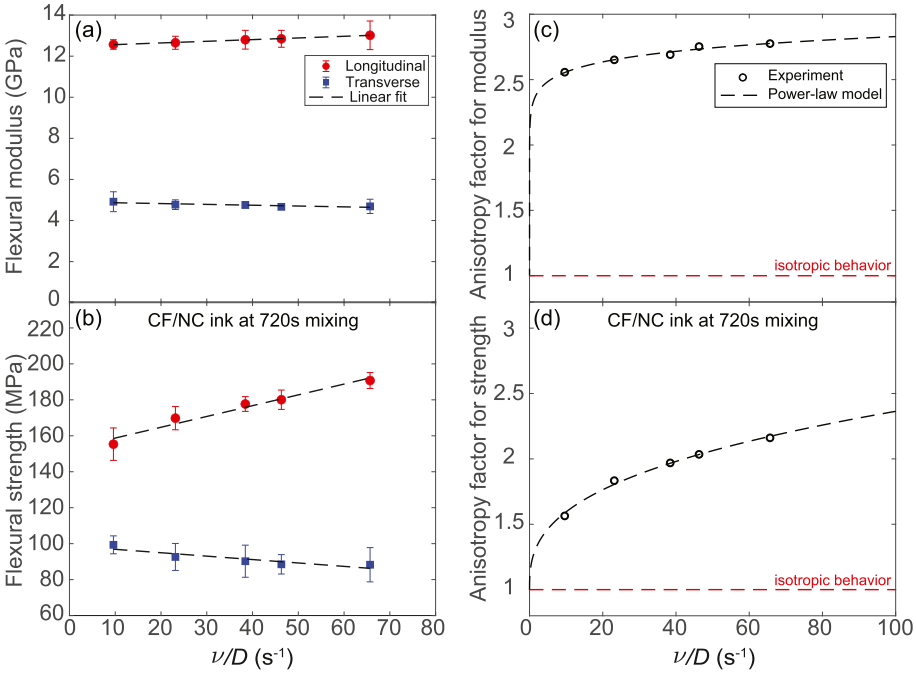

Fig. 11. Flexural properties of longitudinal and transverse CF/NC composites printed with constant mixing time (720 s) and varying ν/D ratios: (a) Flexural modulus and (b) flexural strength. (c) and (d) Corresponding master curves of mechanical anisotropy as a function of ν/D ratio.

$$\chi_2 = \int_{L_{min}}^{L_c} \left[L^2 \Big/ \left(2L_c a^{-1/b} \Gamma[(1/b)+1] \right) \right] abL^{b-1} \exp\left[-aL^b\right] dL + \int_{L_c}^{L_{max}} \left(L \Big/ \left(a^{-1/b} \Gamma[(1/b)+1] \right) \right) (1-(L_c/2L)) abL^{b-1} \exp\left[-aL^b\right] dL \quad (8)$$

From the FLDs of the CF/NC inks in Fig. 4a, $L_{min} = 5\,x\,10^{-6}$m and $L_{max} = 3\,x\,10^{-3}$ m. Based on the fitted Weibull parameters for different mixing times and CF contents (Table 2), k is assumed to be constant for any given volume fraction of fibers and any mixing time, while λ is assumed to decrease linearly with both mixing time and fiber volume fraction (see Fig. S7 and Table S2). Using these assumptions, χ_2 can be calculated as a function of mixing time. For the present set of experiments (V_f = 9.15 *vol*%), k = 2.55, and $\lambda = -0.0003t + 0.513$(in mm), where t is the mixing time (Table S2). Based on these inputs, χ_2 is plotted in Fig. 10a. Computed χ_2 values are 0.64, 0.61, 0.57 and 0.53 for mixing times of 180 s, 360 s, 540 s and 720 s, respectively. Additionally, the percentage of fibers that are above L_c are 40.7%, 39%, 32% and 25.6% for the mixing times of 180 s, 320 s, 540 s, and 720 s, respectively.

Using these values for χ_2 and the fiber and matrix properties summarized in Table 5, experimental strength values are plotted in Fig. 10b along with model predictions for a range of χ_1 values. The model predictions are in good agreement with present range of experimental results when χ_1 = 0.65. Although the FLD clearly has an effect on the strength of the printed composites, the model predictions show that substantially greater gains in strength may be accomplished by increasing χ_1 through greater alignment of fibers along the loading direction. This will be addressed in the following section.

3.8. Mechanical anisotropy

To investigate the effect of nozzle size (D), print speed (ν), and print path orientation on the mechanical anisotropy in printed epoxy/CF composites, two sets of flexural specimens were printed, one with the

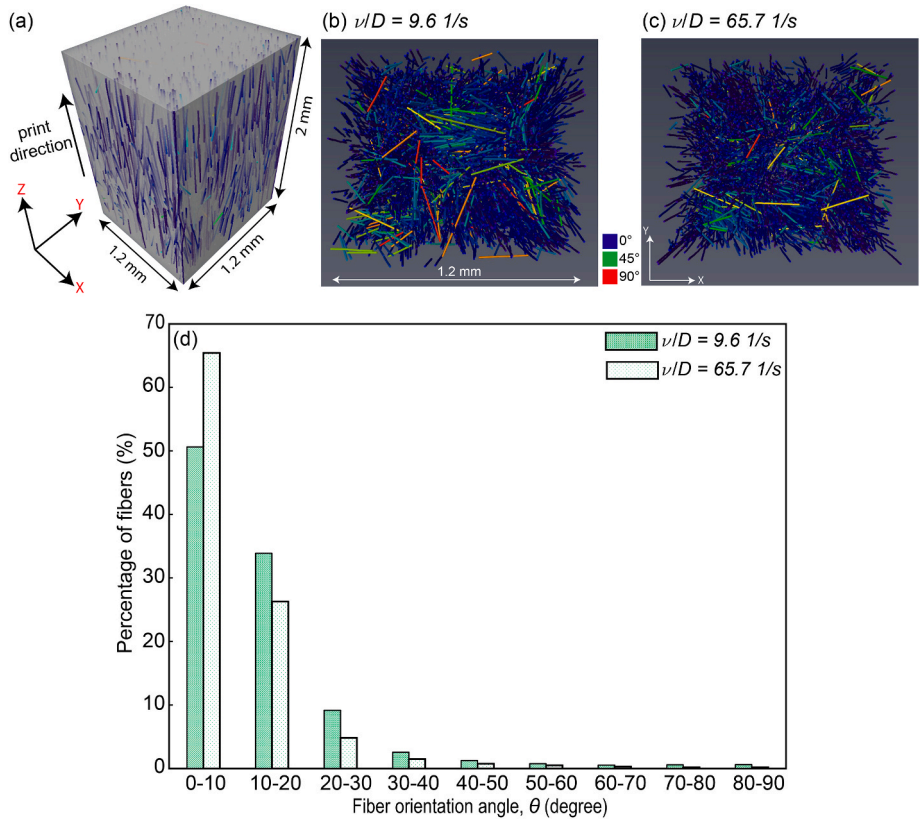

Fig. 12. (a) xCT reconstructions showing the scanned domain of the printed specimen and the coordinate system used. (b–c) X-ray computed tomography scan data for the printed composites with $\nu/D = 9.6\ s^{-1}$ and $\nu/D = 65.7\ s^{-1}$, respectively, with fibers colored by their angle with the Z-axis (i.e., print direction).(d) Histogram of fiber orientation calculated from xCT reconstructions.

print path oriented along (longitudinal) the long dimension of the specimen, and another oriented transverse to the long dimension of the specimen (Fig. S3). These were printed with varying combinations of nozzle size and translation print speed (see Table 4). Only the CF/NC ink at 720s mixing time was chosen to print the composites, since this formulation possessed the most favorable printing behavior. Fig. 11 displays plots of the flexural properties as a function of the print speed over the nozzle diameter (ν/D).

The longitudinal samples display a slight increase in the flexural modulus with increasing ν/D ratio with values ranging from 12.57 GPa to 13.02 GPa, for $\nu/D = 9.6\ s^{-1}$ and $\nu/D = 65.7\ s^{-1}$, respectively (Fig. 11a). Conversely, the transverse samples show a slight decrease in the flexural modulus, with values ranging from 5.0 GPa to 4.7 GPa, for $\nu/D = 9.6\ s^{-1}$ and $\nu/D = 65.7\ s^{-1}$, respectively. The ν/D ratio has a more pronounced effect on the strength of the printed CF/NC composites. The longitudinal strength increases linearly with increasing ν/D ratio from 155.3 MPa up to 190.7 MPa for $\nu/D = 9.6\ s^{-1}$ and $\nu/D = 65.7\ s^{-1}$, respectively. The transverse strength, on the other hand, decreases linearly from 99.3 MPa down to 88.3 MPa for $\nu/D = 9.6\ s^{-1}$ and $\nu/D = 65.7\ s^{-1}$, respectively (Fig. 11b). This increase or decrease in the mechanical strength with increasing ν/D ratio is mainly attributed to the improvement of fiber alignment along the print direction, which is highly influenced by the shear forces that fibers experience during the deposition process [18]. All flexural measurements are summarized in Table 4.

The ratio of the longitudinal to transverse mechanical property can be utilized to define an anisotropy factor (ψ), following [18]. The anisotropy factor for modulus ranges from 2.55 to 2.77 (Fig. 11c), while the anisotropy factor for strength ranges from 1.56 to 2.16 (Fig. 11d) with increasing ν/D ratio. Additionally, the two-parameter power-law model proposed in Ref. [18] is used to fit the anisotropy data:

$$\psi = 1 + A\ (\nu/D)^B \tag{9}$$

where A and B are fitting parameters computed using non-linear regression. The computed values of A and B for this material system are 1.33 and 0.07 for modulus, and 0.26 and 0.36 for strength, respectively (Table S3). The model predictions are plotted along with the data points in Fig. 11c and d. In addition, a comparison between the anisotropy data of the current CF/NC material system and both the NC- and SiC-based material systems investigated in our earlier work [18] is shown in Fig. S8. These characteristic master curves (Fig. 11c,d and Fig. S8), which are highly dependent on the ink viscosity, the morphology of filler materials and nozzle geometry [18], can be employed to guide the optimal selection of nozzle size and print speed.

These results highlight and corroborate inferences made from the composite model presented in section 3.7: for the epoxy/CF composites studied here, the strength of the composite is more sensitive to the extent of alignment of the short fibers than it is to the length distribution of the fibers. Because shorter fibers lead to markedly better printing behavior, which enables printing with smaller nozzles or at higher speeds, it appears that higher fiber alignment, and thus higher mechanical properties can be achieved when inks are mixed for longer times. The relationship between fiber orientation and print parameters is evaluated in the following section.

3.9. Fiber orientation distribution

The improvements in mechanical properties with increasing ν/D ratio discussed in section 3.8 is attributed to increased fiber alignment in the printed composite. Similar trends in the flexural strength and flexural modulus have also been documented in printed epoxy composites containing either NC or a combination of NC and SiC microfibers [18]. In

Table 6
Fiber orientation measurements.

	$\nu/D = 9.6$ 1/s		$\nu/D = 65.7$ 1/s	
Orientation angle, θ (degree)	Fiber count	Frequency (%)	Fiber count	Frequency (%)
0-10	3147	50.63	3723	65.44
10-20	2106	33.88	1495	26.28
20-30	569	9.15	274	4.82
30-40	160	2.57	84	1.48
40-50	78	1.25	43	0.76
50-60	48	0.77	29	0.51
60-70	33	0.53	17	0.30
70-80	37	0.60	12	0.21
80-90	38	0.61	12	0.21
Total fiber counts	6216	100%	5689	100%

that work, microfiber alignment was observed with scanning electron microscopy (SEM) and quantified for the NC using small/wide angle x-ray-scattering (SAXS/WAXS) through Herman's orientation parameter. To quantify the orientation of CF for the present study, high-resolution xCT was conducted on CF/NC composites printed at $\nu/D = 9.6\ s^{-1}$ and $\nu/D = 65.7\ s^{-1}$ with a mixing time of 720s. The scanned domain comprises a 1.2 mm × 1.2 mm x 2 mm prism, with the longer dimension oriented parallel to the print direction (Fig. 12a). After segmentation and analysis, fibers were color-coded by their angle to the print direction to give a visual representation of orientation (Fig. 12b and c). Fibers oriented at 0° are represented by dark blue color, at 45° with green, and at 90° with red color. Qualitatively, it is apparent that fiber alignment is higher in the composite printed at $\nu/D = 65.7\ s^{-1}$ compared to the composite at $\nu/D = 9.6\ s^{-1}$, as indicated by larger number of fibers with dark blue color (Fig. 12c).

A histogram of fiber orientation for each sample (Fig. 12d) quantifies the increase in fiber alignment with print speed. For example, 65% of fibers are oriented within 0–10° of the print direction for the faster print speed, whereas only 51% of fibers have that orientation for the slower print speed. At greater mis-orientation angles, the trend is reversed, and the sample printed at a slower speed has a higher percentage of fibers at any given orientation. Orientation data and fiber counts are tabulated in Table 6.

4. Summary and conclusions

In this work we have investigated the processability, rheological behavior, and mechanical properties of CF-reinforced epoxy composites for DIW 3D printing. The evolution of the fiber length during ink processing was characterized using a wide range of ink compositions and mixing times. Additionally, we have characterized the effect print parameters on mechanical anisotropy and fiber orientation in the printed composites. The key findings of this work can be summarized as follows:

- Fiber length decreases with increasing mixing time and CF content for epoxy/CF DIW composite inks. The incorporation of a rheology-modifier, such as NC platelets, into CF-filled inks allows longer fibers survive the mixing process for longer times. It was found that the FLD can be fit reasonably well using a two-parameter Weibull-type distribution function.
- Mixing time has a significant effect on the rheological properties of both epoxy/NC and CF/NC inks. Both the storage modulus and the shear yield stress of these inks decrease with increasing mixing time, while the apparent viscosity and shear-thinning behavior appear to be independent of mixing time.
- The flexural strength of the printed CF/NC composites decreases with increasing mixing time as a result of decreased fiber length, while the flexural modulus is independent of mixing time.
- Longer mixing time and shorter fibers lead to improved printing behavior and smoother printed surfaces.
- The composite model developed by Fu and Lauke that incorporates FLD and FOD to predict composite strength provides a good fit for the flexural strength of the specific composite formulation studied in this work. .
- Smaller nozzle sizes and higher print speeds lead to greater mechanical anisotropy in the printed CF/NC composites and better properties along the print direction. This is attributed to better alignment of fibers that was quantified using xCT measurements.
- For the materials and print parameters probed in this study, better mechanical properties were achieved by printing inks with shorter fibers at higher speeds or out of finer nozzles compared to inks containing longer fibers printed at lower speeds or out of larger nozzles.

CRediT authorship contribution statement

Nadim S. Hmeidat: Conceptualization, Methodology, Investigation, Validation, Software, Data curation, Formal analysis, Writing – original draft, Writing – Review and Editing, Visualization. **Daniel S. Elkins:** Methodology, Investigation, Data curation, Writing – Review and Editing. **Hutchison R. Peter:** Investigation, Data curation. **Vipin Kumar:** Methodology, Software, Writing – Review and Editing. **Brett G. Compton:** Conceptualization, Supervision, Software, Writing – Review and Editing, Project administration, Funding acquisition.

Declaration of competing interest

The authors declare that they have no known competing financial interests or personal relationships that could have appeared to influence the work reported in this paper.

Acknowledgments

This research was supported through funding from NSF under grant no. CMMI-1825815, and Honeywell Federal Manufacturing and Technologies through Contract DE-NA0002839, managed by Dr. Eric Eastwood, Mr. Steven Patterson, and Dr. Jamie Messman. NSH and BGC would like to acknowledge partial support from the Tennessee Higher Education Commission (THEC) Center for Materials Processing. VK would like to acknowledge support by the US Department of Energy, Office of Energy Efficiency and Renewable Energy, Advanced Manufacturing Office, under contract DE-AC05- 00OR22725 with UT-Battelle, LLC.

Appendix A. Supplementary data

Supplementary data to this article can be found online at https://doi.org/10.1016/j.compositesb.2021.109122.

References

[1] Kokkinis D, Schaffner M, Studart AR. Multimaterial magnetically assisted 3D printing of composite materials. Nat Commun 2015;6:8643.
[2] Rocha VG, et al. Direct ink writing advances in multi-material structures for a sustainable future. J Mater Chem 2020;8(31):15646–57.
[3] Liu J, et al. High thermal conductive epoxy based composites fabricated by multi-material direct ink writing. Compos Appl Sci Manuf 2020;129:105684.
[4] Friedrich L, et al. Acoustic control of microstructures during direct ink writing of two-phase materials. Sensor Actuator Phys 2017;268:213–21.
[5] Collino RR, et al. Deposition of ordered two-phase materials using microfluidic print nozzles with acoustic focusing. Extreme Mechanics Letters 2016;8:96–106.
[6] Melchert DS, et al. Flexible conductive composites with programmed electrical anisotropy using acoustophoresis. Advanced Materials Technologies; 2019. p. 1900586.
[7] Technologies, A.C.F.o.A.M. and A.C.F.o.A.M.T.S.F.o. Terminology. Standard terminology for additive manufacturing technologies. ASTM International; 2012.
[8] Duty CE, et al. Structure and mechanical behavior of big area additive manufacturing (BAAM) materials. Rapid Prototyp J 2017;23(1):181–9.
[9] Love LJ, et al. The importance of carbon fiber to polymer additive manufacturing. J Mater Res 2014;29(17):1893.

[10] Tekinalp HL, et al. Highly oriented carbon fiber–polymer composites via additive manufacturing. Compos Sci Technol 2014;105:144–50.
[11] van de Werken N, et al. Additively manufactured carbon fiber-reinforced composites: state of the art and perspective. Additive Manufacturing 2020;31:100962.
[12] Compton BG, Lewis JA. 3D-printing of lightweight cellular composites. Adv Mater 2014;26(34):5930–5.
[13] Nawafleh N, Celik EJAM. Additive manufacturing of short fiber reinforced thermoset composites with unprecedented mechanical performance 2020;33:101109.
[14] Pierson H, et al. Mechanical properties of printed epoxy-carbon fiber composites. Experimental Mechanics; 2019. p. 1–15.
[15] Pack RC, et al. Carbon fiber and syntactic foam hybrid materials via core–shell material extrusion additive manufacturing. Advanced Materials Technologies; 2020. p. 2000731.
[16] Raney JR, et al. Rotational 3D printing of damage-tolerant composites with programmable mechanics. Proc Natl Acad Sci Unit States Am 2018;115(6):1198–203.
[17] Zhong W, et al. Short fiber reinforced composites for fused deposition modeling. Mater Sci Eng, A 2001;301(2):125–30.
[18] Hmeidat NS, et al. Mechanical anisotropy in polymer composites produced by material extrusion additive manufacturing. Additive Manufacturing 2020;34:101385.
[19] Grejtak T, et al. Whisker orientation controls wear of 3D-printed epoxy nanocomposites. Additive Manufacturing; 2020. p. 101515.
[20] Weng Z, et al. Mechanical and thermal properties of ABS/montmorillonite nanocomposites for fused deposition modeling 3D printing. Mater Des 2016;102:276–83.
[21] Hmeidat NS, Kemp JW, Compton BG. High-strength epoxy nanocomposites for 3D printing. Compos Sci Technol 2018;160:9–20.
[22] Johnson KJ, et al. In operando monitoring of dynamic recovery in 3D printed thermoset nanocomposites by XPCS. Langmuir 2019;35(26):8758–68.
[23] Trigg EB, et al. Revealing filler morphology in 3D-printed thermoset nanocomposites by scanning microbeam X-ray scattering. Additive Manufacturing 2021;37:101729.
[24] Compton BG, et al. Electrical and mechanical properties of 3D-printed graphene-reinforced epoxy. J Occup Med 2018;70(3):292–7.
[25] Haney R, et al. Printability and performance of 3D conductive graphite structures. Additive Manufacturing; 2020. p. 101618.
[26] Shofner M, et al. Nanofiber-reinforced polymers prepared by fused deposition modeling. J Appl Polym Sci 2003;89(11):3081–90.
[27] Compton BG, et al. Mechanical and thermal properties of 3D-printed epoxy composites reinforced with boron nitride nanobarbs. MRS Communications 2021:1–6.
[28] Fu S-Y, Lauke B. Effects of fiber length and fiber orientation distributions on the tensile strength of short-fiber-reinforced polymers. Compos Sci Technol 1996;56(10):1179–90.
[29] Fu S-Y, et al. Tensile properties of short-glass-fiber-and short-carbon-fiber-reinforced polypropylene composites. Compos Appl Sci Manuf 2000;31(10):1117–25.
[30] Ning F, et al. Additive manufacturing of carbon fiber reinforced thermoplastic composites using fused deposition modeling. Compos B Eng 2015;80:369–78.
[31] Calvert P, Lin TL, Martin H. Extrusion freeform fabrication of chopped-fibre reinforced composites. High Perform Polym 1997;9(4):449–56.
[32] Peng J, Lin TL, Calvert P. Orientation effects in freeformed short-fiber composites. Compos Appl Sci Manuf 1999;30(2):133–8.
[33] Malek S, et al. Lightweight 3D cellular composites inspired by balsa. Bioinspiration Biomimetics 2017;12(2):026014.
[34] Heidari-Rarani M, Rafiee-Afarani M, Zahedi A. Mechanical characterization of FDM 3D printing of continuous carbon fiber reinforced PLA composites. Compos B Eng 2019;175:107147.
[35] Goh G, et al. Additively manufactured continuous carbon fiber-reinforced thermoplastic for topology optimized unmanned aerial vehicle structures. Compos B Eng 2021;216:108840.
[36] Goh GD, et al. Process-structure-property of additively manufactured continuous carbon fiber reinforced thermoplastic: an investigation of mode I interlaminar fracture toughness. Mech Adv Mater Struct 2020:1–13.
[37] Wang Z, et al. Mechanical and self-monitoring behaviors of 3D printing smart continuous carbon fiber-thermoplastic lattice truss sandwich structure. Compos B Eng 2019;176:107215.
[38] Caminero M, et al. Interlaminar bonding performance of 3D printed continuous fibre reinforced thermoplastic composites using fused deposition modelling. Polym Test 2018;68:415–23.
[39] Damodaran V, et al. Improving the Mode-II interlaminar fracture toughness of polymeric matrix composites through additive manufacturing. Mater Des 2018;157:60–73.
[40] Valvez S, et al. 3D printed continuous carbon fiber reinforced PLA composites: a short review. Procedia Structural Integrity 2020;25:394–9.
[41] Hao W, et al. Preparation and characterization of 3D printed continuous carbon fiber reinforced thermosetting composites. Polym Test 2018;65:29–34.
[42] He X, et al. 3D printing of continuous fiber-reinforced thermoset composites. Additive Manufacturing 2021;40:101921.
[43] Kanarska Y, et al. Fiber motion in highly confined flows of carbon fiber and non-Newtonian polymer. J Non-Newtonian Fluid Mech 2019;265:41–52.
[44] Lewicki JP, et al. 3D-printing of meso-structurally ordered carbon fiber/polymer composites with unprecedented orthotropic physical properties. Sci Rep 2017;7:43401.
[45] Ennis BL, et al. Evaluation of low-cost carbon fiber materials for use in wind turbine blade design seminar. Albuquerque, NM (United States): Sandia National Lab.(SNL-NM); 2019.
[46] International A. Standard test methods for flexural properties of unreinforced and reinforced plastics and electrical insulating materials. ASTM International; 2010.
[47] Kumar V, et al. High-performance molded composites using additively manufactured preforms with controlled fiber and pore morphology. Additive Manufacturing 2021;37:101733.
[48] Alwekar S, et al. Melt extruded versus extrusion compression molded glass-polypropylene long fiber thermoplastic composites. Compos Appl Sci Manuf 2021:106349.
[49] Yang D, et al. Fibre flow and void formation in 3D printing of short-fibre reinforced thermoplastic composites: an experimental benchmark exercise. Additive Manufacturing; 2020. p. 101686.
[50] Chin WK, Liu HT, Lee YD. Effects of fiber length and orientation distribution on the elastic modulus of short fiber reinforced thermoplastics. Polym Compos 1988;9(1):27–35.
[51] Takahashi K, Choi N-S. Influence of fibre weight fraction on failure mechanisms of poly (ethylene terephthalate) reinforced by short-glass-fibres. J Mater Sci 1991;26(17):4648–56.
[52] Ularych F, et al. Empirical relations of the mechanical properties of polyamide 6 reinforced with short glass fibers. Polym Compos 1993;14(3):229–37.
[53] Siqueira G, et al. Cellulose nanocrystal inks for 3D printing of textured cellular architectures. Adv Funct Mater 2017;27(12):1604619.
[54] Wei TS, et al. 3D printing of customized li-ion batteries with thick electrodes. Adv Mater 2018;30(16):1703027.
[55] Yasmin A, Abot JL, Daniel IM. Processing of clay/epoxy nanocomposites by shear mixing. Scripta Mater 2003;49(1):81–6.
[56] Koerner H, et al. Montmorillonite-thermoset nanocomposites via cryo-compounding. Polymer 2006;47(10):3426–35.
[57] Azeez AA, et al. Epoxy clay nanocomposites–processing, properties and applications: a review. Compos B Eng 2013;45(1):308–20.
[58] Drummy LF, et al. High-resolution electron microscopy of montmorillonite and montmorillonite/epoxy nanocomposites. J Phys Chem B 2005;109(38):17868–78.
[59] Duty C, et al. What makes a material printable? A viscoelastic model for extrusion-based 3D printing of polymers. J Manuf Process 2018;35:526–37.
[60] Fu S-Y, Lauke B. An analytical characterization of the anisotropy of the elastic modulus of misaligned short-fiber-reinforced polymers. Compos Sci Technol 1998;58(12):1961–72.